J. Fluid Mech. (2006), *vol.* 567, *pp.* 457–475.
doi:10.1017/S0022112006002436 Printed in the United Kingdom

On shallow-water wakes: an analytical study

By M. E. NEGRETTI[1], G. VIGNOLI[2], M. TUBINO[2] AND M. BROCCHINI[3]

[1]Institute for Hydromechanics, University of Karlsruhe, Germany
[2]Department of Civil and Environmental Engineering, University of Trento, Italy
[3]Department of Environmental Engineering, University of Genova, Italy

(Received 7 October 2005 and in revised form 22 May 2006)

Analytical solutions for the characteristic scales of a turbulent wake in shallow flows are presented for two asymptotic cases: in one case, boundary-layer effects dominate whereas in the other, wake effects prevail. The latter case degenerates into the solution valid for an unbounded two-dimensional wake. These solutions show that the momentum deficit decreases exponentially in the longitudinal direction while the transverse velocity profile reveals a wake region characterized by a reduced velocity deficit compared to that of an unbounded wake. When wake-turbulence dominates there is a non-uniform turbulent viscosity in the longitudinal direction. These analytical solutions are compared with experimental data showing good agreement.

1. Introduction

Free turbulence has been widely investigated in the last forty years. A number of analytic solutions describing phenomena such as wakes, jets and mixing layers are well established and provide a solid foundation for further studies on small-scale properties of turbulent flows (Bearman 1967; Tennekes & Lumley 1977). The common feature of free turbulence is the slow longitudinal flow variability as compared to the variability in the transverse direction. In some cases of environmental relevance, wakes develop in a confined ambient where the flow can be treated as shallow. Basic knowledge of shallow wakes is still limited: unlike the case of unbounded wakes, no analytical solutions for the fundamental variables (e.g. velocity deficit, transverse dimension of the wake and wake velocity profile) are yet available.

In nature, shallow flows are ubiquitous, and important examples include nearshore waters, rivers, the lower layer of the atmosphere (see figure 1) and the upper layers of the oceans. Shallow-wake flows are observed at different scales, for example downstream of invested structures such as columns of bridges, coastal protection structures (e.g. piers interrupting longshore currents), and islands immersed in oceanic currents such as the Gulf Stream. In this case, the slow variability of the flow in the longitudinal direction is preserved, while the vorticity production is not only generated by the presence of the wake, but also by bottom friction (Grubisic, Smith & Schar 1995).

In shallow flows, friction plays a role on the stability of the wake similar to viscosity in the transition from laminar to turbulent flow. Instabilities can be generated, which sometimes lead to the production of two-dimensional coherent structures (see Jirka 2001). Schlichting & Gersten (2000) investigated the asymptotic behaviour

FIGURE 1. An example of a shallow wake. Aerial picture of the Canary Islands (NASA). The lower layer of the atmosphere shows typical features of a shallow flow. A von Kármán vortex street with large coherent structures downstream of the islands can be clearly seen thanks to the presence of clouds.

of boundary-layer solutions far downstream of their inception. The large-distance expansion for wakes behind two-dimensional bodies has been given by Tollmien (1931). Berger (1971) extended similar solutions in the near-inception region. Hinze (1975) and Tennekes & Lumley (1977) were able to obtain an analytical expression for the transverse velocity profiles of free turbulent wakes. Furthermore, Schlichting & Gersten (2000) showed that a class of turbulent unbounded two-dimensional flows, which satisfy self-preservation, always lead to the same form of the differential equation for the transverse velocity profile, whose solution is the well-known Gaussian profile (see also Pope 2000). Tennekes & Lumley (1977) and Schlichting & Gersten (2000) also compared these results with experimental data and found good agreement.

Similar to other two-dimensional flows, the transverse distribution of the velocity deficit in shallow wakes induced by various obstacles has been described using Gaussian distributions (Hinze 1975; Pope 2000), although other functional dependencies, e.g. trigonometrical or even polynomial, have also been proposed (Chen & Jirka 1997; Carmer 2005).

Here we summarize the results of an analytical study of the shallow-water equations aimed at deriving a general expression for the characteristic scales of a shallow wake, i.e. for the velocity deficit, for the transverse dimension of the wake and, finally, for the transverse wake velocity profile including the effect of acceleration due to gravity and bottom friction. Our analytical approach follows closely that of Hinze

(1975), Tennekes & Lumley (1977) and Schlichting & Gersten (2000). Two asymptotic cases are distinguished on the basis of the mechanism of turbulence production. An analytical solution is first derived closing the turbulent shear stress term with an expression for the turbulent viscosity ν_T typical of free turbulence. In the second case, the turbulent viscosity is modelled assuming that the dominant turbulence production mechanism is the no-slip condition at the bottom.

Following closely the route of Tennekes & Lumley (1977) for unbounded wakes, we propose an analytical solution for shallow wakes which can also be used as a suitable basis for stability analysis, like those proposed by Heurre & Monkewitz (1990); Williamson (1996); Socolofsky & Jirka (2004).

Some direct examples where the above solution is useful are related to mixing processes induced by obstacles in shallow flows. For instance, simplified solutions for the transport of pollutants downstream of bridges in rivers or piers in coastal waters and for oceanic nutrients (e.g. plankton, micro-algae, etc.) in the lee of islands can be obtained on the basis of the mean flow structure provided by the present solutions.

In § 2, the problem is formulated, the characteristic length scales which govern the system are presented and a dimensional analysis for the governing equations is performed to simplify the model. The analytical results obtained under the assumption of a constant friction coefficient and the comparison with experimental data (Carmer 2005) are discussed in § 3.3 when free turbulence is dominant (case I), and in § 3.4 when wall turbulence dominates (case II). In § 3.5, a brief comparison of the results for shallow wakes with the results for unbounded wake flows is made. Section 4 summarizes the results and includes some concluding remarks.

2. Formulation of the problem

2.1. *The flow scales*

In a turbulent unbounded wake, two distinct length scales can be identified. The first one, $l(x)$, is the transverse width of the wake from the centreline, which is typically defined as the distance from the centreline, where the velocity deficit becomes a percentage (e.g. 60 %) of the maximal value of the velocity deficit. The second one, L, is the longitudinal scale, which represents the downstream distance over which flow properties, such as the velocity deficit, undergo a sensible variation (see figure 2). A more detailed definition of such a length scale is given in § 3.1.

The study of free turbulence is, generally, based on an order-of-magnitude analysis of the terms appearing in the equations of motion and in the continuity equation. In the case of turbulent wakes, as confirmed by experimental observations (Tennekes & Lumley 1977), the equation of motion in the longitudinal direction reduces to a balance between longitudinal convection and the transverse flux of the turbulent shear stress.

If the flow under investigation is shallow, another characteristic length scale can be defined, i.e. the water depth h_0. In this case, the above length scales range as follows:

$$h_0 \ll l \ll L.$$

Further scales are also required to characterize velocity and turbulent quantities. In turbulent wakes an obvious scale is provided by the ambient velocity u_∞, which is used for the mean flow in the streamwise direction. Another scale is introduced for the cross-stream variation of the same velocity component, namely the 'velocity deficit' $u_s (\ll u_\infty)$.

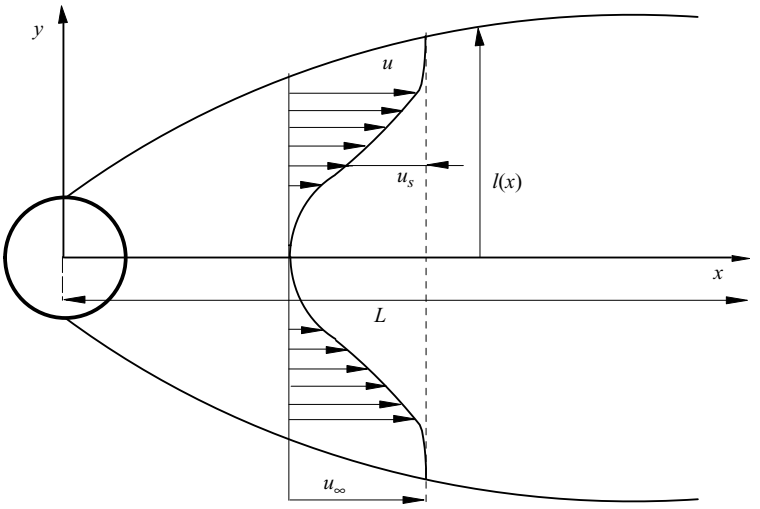

FIGURE 2. Sketch of a wake downstream of an obstacle with the notation in use. $l(x)$ is the transverse width of the wake from the centreline, L is the longitudinal characteristic scale, u is the instantaneous velocity, u_∞ is the ambient velocity in the longitudinal direction and u_s is the velocity deficit with respect to the ambient value.

The order of magnitude of the instantaneous streamwise velocity $u(x, y) = u_\infty - u_s$ is $O(u) = u_\infty$, while those of the velocity gradients are $\partial u/\partial y = O(u_s/l)$ and $\partial u/\partial x = O(u_s/L)$; furthermore, the continuity equation provides the following estimate for the cross-stream velocity component: $v = O(u_s l/L)$.

Shallow flows, with small vertical gradients, are typically averaged over the depth h of scale h_0. This is much smaller than the planimetric scale l and this assumption allows us to evaluate the scale for the vertical component of the velocities:

$$w_0 = \frac{h_0}{l} u_\infty, \qquad \frac{h_0}{l} \ll 1. \tag{2.1}$$

In addition, a scale for the Reynolds stresses is introduced in the following form

$$-\overline{u'v'} = \overline{u'^2} = \overline{v'^2} = O(w^2)$$

where w is assumed to be proportional to the ambient velocity u_∞ through a constant k.

2.2. *The model equations*

Following a standard procedure used for shallow flows, we pose the problem in terms of the depth-averaged mass conservation equation and Reynolds equations. Bottom friction is included, while the viscous term is neglected, since, for large enough Reynolds numbers, turbulent friction dominates. The above equations read:

$$\frac{\partial h}{\partial t} + \frac{\partial (h\overline{u})}{\partial x} + \frac{\partial (h\overline{v})}{\partial y} = 0, \tag{2.2}$$

$$\frac{\partial \overline{u}}{\partial t} + \overline{u}\frac{\partial \overline{u}}{\partial x} + \overline{v}\frac{\partial \overline{u}}{\partial y} + g\frac{\partial h}{\partial x} - gi_F + \frac{f}{8h}\overline{u}\sqrt{\overline{u}^2+\overline{v}^2} + \frac{1}{h}\left[\frac{\partial}{\partial x}(h\overline{u'u'}) + \frac{\partial}{\partial y}(h\overline{u'v'})\right] = 0, \tag{2.3}$$

$$\frac{\partial \overline{v}}{\partial t} + \overline{u}\frac{\partial \overline{v}}{\partial x} + \overline{v}\frac{\partial \overline{v}}{\partial y} + g\frac{\partial h}{\partial y} + \frac{f}{8h}\overline{v}\sqrt{\overline{u}^2+\overline{v}^2} + \frac{1}{h}\left[\frac{\partial}{\partial x}(h\overline{u'v'}) + \frac{\partial}{\partial y}(h\overline{v'v'})\right] = 0. \tag{2.4}$$

Here, $\bar{u}$ and $\bar{v}$ are the components of the depth-averaged velocity vector along x and y respectively, h is the local water depth, g the acceleration due to gravity, f is the Darcy–Weisbach friction parameter, i_F is the longitudinal bed slope and t is time. Moreover, the overbar indicates quantities averaged over the depth and the prime denotes the turbulent fluctuations. The momentum equations can be rewritten in conservative form as follows:

$$\frac{\partial(h\overline{u})}{\partial t}+\frac{\partial(h\overline{u}\overline{u})}{\partial x}+\frac{\partial(h\overline{u}\overline{v})}{\partial y}+\frac{\partial}{\partial x}\left(\frac{gh^2}{2}\right)+\frac{\partial}{\partial x}(h\overline{u'u'})+\frac{\partial}{\partial y}(h\overline{u'v'})=ghi_F-\frac{f}{8}\overline{u}\sqrt{\overline{u}^2+\overline{v}^2}, \tag{2.5}$$

$$\frac{\partial(h\overline{v})}{\partial t}+\frac{\partial(h\overline{u}\overline{v})}{\partial x}+\frac{\partial(h\overline{v}\overline{v})}{\partial y}+\frac{\partial}{\partial y}\left(\frac{gh^2}{2}\right)+\frac{\partial}{\partial x}(h\overline{u'v'})+\frac{\partial}{\partial y}(h\overline{v'v'})=\frac{f}{8}\overline{v}\sqrt{\overline{u}^2+\overline{v}^2}. \tag{2.6}$$

2.3. *The simplified model*

The scaling arguments introduced in the previous subsection allow for simplification of the governing equations (2.2), (2.3) and (2.4). Since $h_0 \ll l \ll L$, $u_s \ll u_\infty$ and $v_\infty = 0$ and assuming steady mean flow, the following estimates can be obtained:

$$u = u_\infty - u_s \sim u_\infty, \quad v = v_\infty + v_s = v_s \ll u_\infty \quad (v_s \ll u_s),$$
$$h = h_\infty - \delta h \sim h_\infty.$$

We also assume the friction factor f to be constant, as it is appropriate for a far-wake flow, where the bottom friction slowly varies in space and a self-similar behaviour is approached (e.g. Negretti 2003). We note that the above approximation does not hold in the near field of wakes with low velocities or high strain rate, as has been shown by the numerical solution of Stansby (2003).

An order of magnitude analysis of terms appearing in the cross-flow equation (2.4) leads to the following estimates:

$$\frac{\partial\overline{v}}{\partial t}+\overline{u}\frac{\partial\overline{v}}{\partial x}+\overline{v}\frac{\partial\overline{v}}{\partial y}+g\frac{\partial h}{\partial y}+\frac{f}{8h}\overline{v}\sqrt{\overline{u}^2+\overline{v}^2}+\frac{1}{h}\left[\frac{\partial}{\partial x}(h\overline{u'v'})+\frac{\partial}{\partial y}(h\overline{v'v'})\right]=0 \tag{2.7}$$

$$0 \quad u_\infty\frac{v_s}{L} \quad v_s\frac{v_s}{l} \quad g\frac{h_s}{l} \quad \frac{f}{8h_\infty}v_s u_\infty \quad \frac{w^2}{L} \quad \frac{w^2}{l}.$$

Hence, at the leading order of approximation, (2.7) reduces to the following balance:

$$g\frac{\partial h}{\partial y}+\frac{1}{h}\frac{\partial}{\partial y}(h\overline{v'v'})=0 \quad\Longrightarrow\quad \frac{\partial}{\partial y}\left(\frac{gh^2}{2}\right)+\frac{\partial}{\partial y}(h\overline{v'v'})=0. \tag{2.8}$$

Formal integration of (2.8) with respect to y and subsequent derivation with respect to x leads to:

$$gh\frac{\partial h}{\partial x}+\frac{\partial(h\overline{v'v'})}{\partial x}=0. \tag{2.9}$$

Substitution into (2.5) gives:

$$\overline{u}\frac{\partial\overline{u}}{\partial x}+\overline{v}\frac{\partial\overline{u}}{\partial y}-gi_F+\frac{f}{8h}\overline{u}\sqrt{\overline{u}^2\overline{v}^2}+\frac{1}{h}\left[\frac{\partial}{\partial x}(h\overline{u'u'}-h\overline{v'v'})+\frac{\partial}{\partial y}(h\overline{u'v'})\right]=0, \tag{2.10}$$

for which the following scaling holds

$$\frac{u_\infty u_s}{L} \quad \frac{u_s v_s}{l} \quad gi_F \quad \frac{f}{8h_\infty}\overline{u}_\infty^2 \quad \frac{w^2}{L} \quad \frac{w^2}{l}. \tag{2.11}$$

The above estimates suggest that the second and the fifth terms in (2.11) can be neglected so that (2.10) reduces to:

$$\frac{\partial(h\overline{uu})}{\partial x} + \frac{\partial}{\partial y}(h\overline{u'v'}) - ghi_F + \frac{f}{8}\overline{u}\sqrt{\overline{u}^2 + \overline{v}^2} = 0. \tag{2.12}$$

Far from the wake zone, i.e. for $y \to \infty$, equation (2.12) reads:

$$-gh_\infty i_F + \frac{f}{8}\overline{u}_\infty^2 = 0. \tag{2.13}$$

Hence, subtracting (2.13) from (2.12), we find:

$$\frac{\partial(h\overline{uu})}{\partial x} + \frac{\partial}{\partial y}(h\overline{u'v'}) + \frac{f}{8}\left(\overline{u}\sqrt{\overline{u}^2 + \overline{v}^2} - \overline{u}_\infty^2\right) + g(h_\infty - h)i_F = 0. \tag{2.14}$$

Simple algebraic manipulations and scaling arguments lead to a simplified expression for the third term appearing in (2.14) which takes the following form:

$$\overline{u}\sqrt{\overline{u}^2 + \overline{v}^2} - \overline{u}_\infty^2 \sim = 2\overline{u}\,(\overline{u} - \overline{u}_\infty)\,.$$

Substituting into (2.14) gives:

$$\frac{\partial(h\overline{uu})}{\partial x} + \frac{\partial}{\partial y}(h\overline{u'v'}) + \frac{f}{4}\,(\overline{u} - \overline{u}_\infty)\,\overline{u} + g(h_\infty - h)i_F = 0. \tag{2.15}$$

Using the steady form of the continuity equation (2.2), the first term of (2.15) can be rewritten as:

$$\overline{u}_\infty \frac{\partial(h\overline{u})}{\partial x} - \frac{\partial(hu_s\overline{u})}{\partial x} = -\overline{u}_\infty \frac{\partial(h\overline{v})}{\partial y} - \frac{\partial(hu_s\overline{u})}{\partial x}. \tag{2.16}$$

Furthermore, integration of (2.15) in the transverse direction with use of (2.16) leads to:

$$-\int_{-\infty}^{\infty} u_\infty \frac{\partial(h\overline{v})}{\partial y}\,\mathrm{d}y - \int_{-\infty}^{\infty} \frac{\partial(hu_s\overline{u})}{\partial x}\,\mathrm{d}y - \int_{-\infty}^{\infty} \frac{f}{4}u_s\overline{u}\,\mathrm{d}y + \int_{-\infty}^{\infty} \frac{\partial}{\partial y}(h\overline{u'v'})\,\mathrm{d}y + g\int_{-\infty}^{\infty}(h_\infty - h)i_F\,\mathrm{d}y = 0. \tag{2.17}$$

One can readily see that the first and the fourth terms appearing in (2.17) vanish because the flow deficit vanishes far from the axis of symmetry. The last integral requires a more detailed analysis. Using the continuity equation and (2.13) we obtain the following estimate:

$$g(h_\infty - h)i_F = gi_F\delta h \sim gi_F\frac{h_\infty u_s}{u_\infty} = \frac{f}{8}u_s(\overline{u} + u_s). \tag{2.18}$$

The second integral in (2.17) can be rewritten as follows:

$$\begin{aligned}\int_{-\infty}^{\infty} \frac{\partial(hu_s\overline{u})}{\partial x}\,\mathrm{d}y &= \int_{-\infty}^{\infty} \frac{\partial[(h_\infty - \delta h)u_s\overline{u}]}{\partial x}\,\mathrm{d}y \sim \int_{-\infty}^{\infty} \frac{\partial[(h_\infty - \frac{h_\infty u_s}{\overline{u}})u_s\overline{u}]}{\partial x}\,\mathrm{d}y \\ &= \frac{\partial}{\partial x}\left[\int_{-\infty}^{+\infty} h_\infty u_s\overline{u}\,\mathrm{d}y + \int_{-\infty}^{+\infty} h_\infty \frac{u_s^2}{u_\infty}\overline{u}\,\mathrm{d}y\right].\end{aligned} \tag{2.19}$$

Using (2.18) and (2.19), equation (2.17) reduces to:

$$\frac{\partial}{\partial x}\left[\int_{-\infty}^{+\infty} h_\infty u_s\overline{u}\,\mathrm{d}y + \int_{-\infty}^{+\infty} h_\infty \frac{u_s^2}{u_\infty}\overline{u}\,\mathrm{d}y\right] = -\frac{f}{8}\left[\int_{-\infty}^{+\infty} u_s\overline{u}\,\mathrm{d}y - \int_{-\infty}^{+\infty} u_s^2\,\mathrm{d}y\right]. \tag{2.20}$$

Finally, neglecting the small contribution associated with terms proportional to u_s^2, equation (2.20) becomes:

$$\frac{\partial}{\partial x}\int_{-\infty}^{\infty} h_\infty u_s \overline{u}\,\mathrm{d}y = -\frac{f}{8h_\infty}\int_{-\infty}^{\infty} h_\infty u_s \overline{u}\,\mathrm{d}y, \tag{2.21}$$

which is the final approximate form of the streamwise momentum equation that is used below.

3. Results and discussion

3.1. *The momentum deficit*

The first novelty introduced by the shallow-water character of the present analysis is in the expression for the wake momentum deficit $\mathscr{M} \equiv \int_{-\infty}^{+\infty} \overline{u} u_s h_\infty \,\mathrm{d}y$. In terms of $\mathscr{M}$, equation (2.21) can be rewritten in the form:

$$\frac{\mathrm{d}\mathscr{M}}{\mathrm{d}x} = -\frac{f}{8h_\infty}\mathscr{M}, \tag{3.1}$$

whose solution is the exponential function:

$$\mathscr{M}(x) = \mathscr{M}_0 \exp\left(-\frac{f}{8h_\infty}x\right), \tag{3.2}$$

where $\mathscr{M}_0$ is the momentum deficit at the initial section. Equation (3.2) is significantly different from the analogous relation derived in the context of free turbulence, where $\mathscr{M}$ stays constant in the x-direction. In shallow wakes, the momentum exchange between the ambient region and the wake zone behind the obstacle is still based on the generation of two-dimensional coherent structures; furthermore, the bottom friction dissipates the turbulent kinetic energy of the wake turbulence though its effect is weaker than in the ambient flow owing to the smaller value of the velocity. As a result, the x-momentum deficit decreases exponentially. Using the rigid-lid assumption, Carmer (2005) derived an integral far-wake model with a momentum deficit equation similar to (3.2) that overestimates the frictional effect by a factor 2. Indeed, equation (2.18) shows that gravity plays an important role, halving the effect of bottom friction.

Equation (3.2) can be reinterpreted in terms of the stability number S

$$S = \frac{f}{4}\frac{D}{h_\infty}$$

which has been used to describe the stability of a shallow flow around an obstacle, like a circular cylinder of diameter D (Chen & Jirka 1995). S represents the ratio between the loss of turbulent kinetic energy due to bed friction and the production of coherent kinetic energy due to lateral shear. Chen & Jirka (1995) have shown experimentally that three different types of wake pattern in shallow-water flows can occur depending on the value of the stability number. For $S < 0.2$, a vortex street-like wake develops, which is the most unstable wake. For $S > 0.5$, a wake with an attached steady bubble develops. The transition case, $0.2 < S < 0.5$, is represented by a wake with an attached unsteady bubble behind the obstacle (see figure 3).

We than obtain

$$\mathscr{M}(x) = \mathscr{M}_0 \exp\left(-\frac{S}{2D}x\right). \tag{3.3}$$

It appears that the more stable the wake (that is, the larger S is) the faster is the decrease of the momentum deficit in the longitudinal direction. This means that in

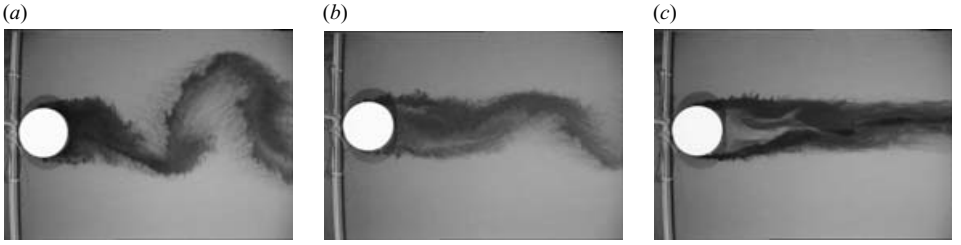

FIGURE 3. Top view (instantaneous photographs) of different wake patterns in shallow flows visualized by dye injected at the upstream cylinder shoulders. Vortex street-like wake (left), unsteady bubble (middle), steady bubble (right). Adapted from Carmer (2005).

a vortex street-like wake, the region affected by a deficit of the velocity can extend further downstream with respect to the case of a wake with a stable bubble.

Equation (3.2) also suggests a suitable definition for the longitudinal length scale L:

$$L \equiv \frac{8h_\infty}{f}. \tag{3.4}$$

Hence, using the dimensionless variables $x_L \equiv x/L$ and $M = \mathscr{M}/\mathscr{M}_0$, equation (3.2) reduces to the simple dimensionless form:

$$M(x_L) = \exp(-x_L). \tag{3.5}$$

3.2. *Dimensional analysis*

A suitable definition of the velocity profile in the cross-stream direction for a shallow-wake flow has been empirically obtained by many authors (see for example Chen & Jirka 1997). Here the attempt is pursued to derive simplified analytical relations for the above velocity profile, for the transverse length scale l and for the velocity deficit u_s, based on the analysis of the order of magnitude of the terms appearing in (2.15), which is now rewritten in the form:

$$\underbrace{\overline{u}\frac{\partial \overline{u}}{\partial x}}_{\text{I}} + \underbrace{\frac{\partial(\overline{u'v'})}{\partial y}}_{\text{II}} + \underbrace{\frac{f}{4h}(\overline{u}-u_\infty)\sqrt{\overline{u}^2+\overline{v}^2}}_{\text{III}} + \underbrace{g\frac{\delta h}{h}i_F}_{\text{IV}} = 0. \tag{3.6}$$

Recalling that the assumption $u_s \ll u_\infty$ is valid within a region sufficiently far from the obstacle, the following scaling holds:

$$\text{I:} \qquad \overline{u}\frac{\partial \overline{u}}{\partial x} \sim u_\infty \frac{u_s}{L} = \frac{h_0}{h_\infty} \times \left(\frac{u_s u_\infty f}{8h_0}\right), \tag{3.7}$$

$$\text{II:} \qquad \frac{\partial \overline{u'v'}}{\partial y} \sim \frac{w^2}{l} = k^2 \frac{h_0}{h_\infty}\frac{L}{l}\frac{u_\infty}{u_s} \times \left(\frac{u_s u_\infty f}{8h_0}\right), \tag{3.8}$$

$$\text{III:} \quad \frac{f}{4h}(\overline{u}-u_\infty)\sqrt{\overline{u}^2+\overline{v}^2} \sim \frac{f}{4h_0}u_s u_\infty = 2 \times \left(\frac{u_s u_\infty f}{8h_0}\right), \tag{3.9}$$

$$\text{IV:} \qquad g\frac{\delta h}{h}i_F \sim g\frac{u_s}{u_\infty}i_F = 1 \times \left(\frac{u_s u_\infty f}{8h_0}\right). \tag{3.10}$$

From this, it follows that terms I, III and IV have the same order of magnitude, while no statement can be made on the size of II. A self-similar solution of equation

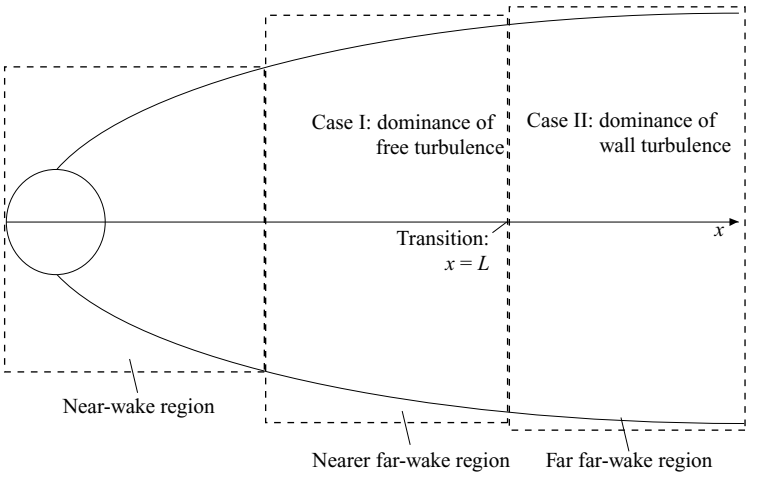

FIGURE 4. Definition of case I (dominance of wake turbulence) and case II (dominance of wall turbulence). The cross-section $x \sim L$ represents the transition from case I to case II.

(3.6) is sought in the form:

$$u_s = u_\infty - u(x, y) = \hat{u}_s \varphi(\zeta) \tag{3.11}$$

where the overline is omitted for simplicity, $\zeta = y/l$ is the transverse coordinate normalized with the local wake width l, and $\varphi(\zeta)$ represents the function which describes the transverse velocity deficit profile. Terms I, III and IV of (3.6) can be given the following form, respectively:

$$u\frac{\partial u}{\partial x} = -u\left[\frac{\mathrm{d}\hat{u}_s}{\mathrm{d}x}\varphi - \frac{\hat{u}_s}{l}\zeta\frac{\mathrm{d}l}{\mathrm{d}x}\frac{\mathrm{d}\varphi}{\mathrm{d}\zeta}\right], \tag{3.12}$$

$$\frac{f}{4h}(u-u_\infty)\sqrt{u^2+v^2} \sim -\frac{f}{4h}u_s u = -\frac{f}{4h_\infty(1-u_s/u_\infty)}u_s u \sim -\frac{f}{4h_\infty}u_\infty u_s, \tag{3.13}$$

$$g\frac{\delta h}{h}i_F = \frac{f}{8h_\infty}u_\infty u_s. \tag{3.14}$$

Substituting (3.12), (3.13) and (3.14) into (3.6) gives:

$$-u\left[\frac{\mathrm{d}\hat{u}_s}{\mathrm{d}x}\varphi - \frac{\hat{u}_s}{l}\zeta\frac{\mathrm{d}l}{\mathrm{d}x}\frac{\mathrm{d}\varphi}{\mathrm{d}\zeta}\right] + \frac{\partial(\overline{u'v'})}{\partial y} = \frac{f}{8h_\infty}\hat{u}_s u_\infty \varphi. \tag{3.15}$$

The solution of (3.15) requires the introduction of a suitable closure relationship for the turbulent term $\partial\overline{u'v'}/\partial y$, which is given here through a simple diffusive model, such that $-\overline{u'v'} = \nu_t(\partial u/\partial y)$.

As pointed out in § 1, in shallow wakes two distinct mechanisms can be responsible for turbulence production. Hence, in the following, two asymptotic cases are treated. In case I, it is assumed that turbulence is essentially caused by the development of the wake (this occurs in the nearer far wake). In case II, bottom friction dominates turbulence production, which is a configuration occurring in the extreme far-wake region. The distinction between the two cases can be set in terms of the dimensionless variable x_L, such that the former occurs in the asymptotic limit $x_L \ll 1$, while the latter corresponds to $x_L \gg 1$. As a consequence, a shallow wake transits from case I to case II as it develops downstream (see figure 4), since the wake exponentially decreases while the effect of bottom friction remains nearly constant.

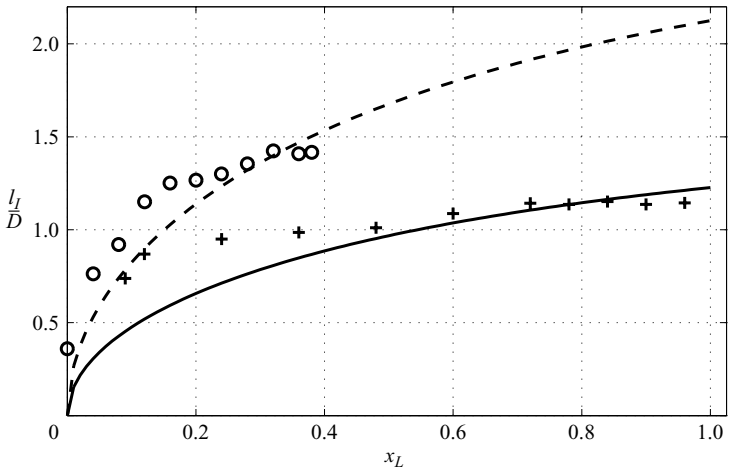

FIGURE 5. Transverse dimension of the wake normalized with the cylinder diameter (cf. equation (3.31)). Analytical solution (dashed line, $S = 0.02$; continuous line, $S = 0.06$) in the case of free turbulence dominance (case I) is compared with the experimental data of Carmer (2005): $S = 0.02$ (circles); $S = 0.06$ (crosses).

3.3. *Self-similarity and mean velocity profile: dominance of free turbulence (case I)*

In this case, it is assumed that turbulence production by bottom friction is negligible compared to the turbulence generated by the wake. This is expected to happen in the nearer far-wake region i.e. for $x_L \ll 1$ (see figures 4 and 5). The turbulent viscosity ν_t is then evaluated using the typical closure law for free turbulence:

$$\nu_t = \kappa \hat{u}_s l \tag{3.16}$$

where κ is a proportionality constant. Hence, the momentum flux due to transverse velocity fluctuations can be rewritten as:

$$-\frac{\partial(\overline{u'v'})}{\partial y} = -\frac{1}{l}\frac{\partial}{\partial \zeta}\left[\frac{\nu_t}{l}\frac{\partial u_s}{\partial \zeta}\right] = -\frac{1}{l}\kappa \hat{u}_s^2 \varphi''. \tag{3.17}$$

Using this expression and approximating the velocity in the wake u with the ambient velocity u_∞, equation (3.15) becomes:

$$-\left[\frac{u_\infty l}{\hat{u}_s^2}\frac{\mathrm{d}\hat{u}_s}{\mathrm{d}x} + fl\frac{u_\infty}{\hat{u}_s}\right]\varphi + \left[\frac{u_\infty}{\hat{u}_s}\frac{\mathrm{d}l}{\mathrm{d}x}\right]\zeta\frac{\mathrm{d}\varphi}{\mathrm{d}\zeta} = -\kappa\frac{\mathrm{d}^2\varphi}{\mathrm{d}\zeta^2}. \tag{3.18}$$

Self-similarity requires that the normalized profiles of the velocity deficit and of the Reynolds stress must be the same for all x, which implies that the coefficients in square brackets must be constant:

$$\frac{u_\infty l}{\hat{u}_s^2}\frac{\mathrm{d}\hat{u}_s}{\mathrm{d}x} + \frac{u_\infty f l}{8h_\infty}\frac{1}{\hat{u}_s} = n, \tag{3.19}$$

$$\frac{u_\infty}{\hat{u}_s}\frac{\mathrm{d}l}{\mathrm{d}x} = m. \tag{3.20}$$

To proceed with an analytical treatment of the problem, a further relationship between the two constants n and m is obtained on the basis of dimensional arguments.

Dividing (3.19) by (3.20) it follows that:

$$\frac{\dfrac{u_\infty l \hat{u}_s}{\hat{u}_s^2 L}}{\dfrac{u_\infty l}{\hat{u}_s L}} + \frac{\dfrac{u_\infty f l}{\hat{u}_s 8h_\infty}}{\dfrac{u_\infty l}{\hat{u}_s L}} = \frac{n}{m}. \tag{3.21}$$

Both terms on the left-hand side of (3.21) have size $O(1)$, hence the two constants appearing at the right-hand side are of the same order of magnitude. Therefore, with no loss of generality, we can be set $|n| = |m|$. Furthermore, the first term on the left-hand side of (3.19) contains the derivative of u_s with respect to x, which is expected to be negative because the deficit decreases with increasing distance from the obstacle. On the contrary, the left-hand side of (3.20) is positive, since the transverse dimension of the wake l increases with increasing distance from the obstacle. This implies that n and m must have opposite signs and the following relationship can be introduced:

$$\frac{m}{n} = -1. \tag{3.22}$$

Suitability of the above assumption is verified *a posteriori* through comparison of the analytical solution with experimental data.

From (3.20) it follows that

$$\frac{\mathrm{d}l}{\mathrm{d}x} = \frac{m}{u_\infty}\hat{u}_s \Rightarrow \frac{\mathrm{d}^2 l}{\mathrm{d}x^2} = \frac{m}{u_\infty}\frac{\mathrm{d}\hat{u}_s}{\mathrm{d}x}. \tag{3.23}$$

Substituting (3.23) into (3.19), an ordinary differential equation for the function $l(x)$ is obtained, which reads:

$$\frac{\mathrm{d}^2 l}{\mathrm{d}x^2} l + \frac{f}{8h_\infty}\frac{\mathrm{d}l}{\mathrm{d}x} l + \left(\frac{\mathrm{d}l}{\mathrm{d}x}\right)^2 = 0. \tag{3.24}$$

Note that the structure of the differential governing equation has been highly simplified in view of the assumption (3.22). From a mathematical point of view, this means that the above assumption leads to a restriction of the family group of solutions for the governing equation. From a physical point of view, dimensional analysis suggests that only these solutions are of interest.

The solution of (3.24) is:

$$l(x) = \sqrt{\frac{16Ah_\infty}{f}[1 - \exp(-x_L] - B)}, \tag{3.25}$$

from which the solution for the velocity deficit is readily obtained in the form

$$\hat{u}_s(x) = u_\infty \frac{A}{m} \frac{\exp(-x_L)}{\sqrt{16Ah_\infty/f\,[1 - \exp(-x_L)] - B}}. \tag{3.26}$$

Use of the variable ζ, defined in terms of the conventional length l, does not allow us to set the boundary conditions directly, so the integration constants A and B must be determined through a different approach. To this purpose we observe that in the case of a smooth bottom ($f \to 0$), the structure of (3.25) should tend to the solution obtained by Tennekes & Lumley (1977) in the case of free turbulence, i.e. to:

$$l = F\sqrt{\frac{D}{2}}\sqrt{x}, \tag{3.27}$$

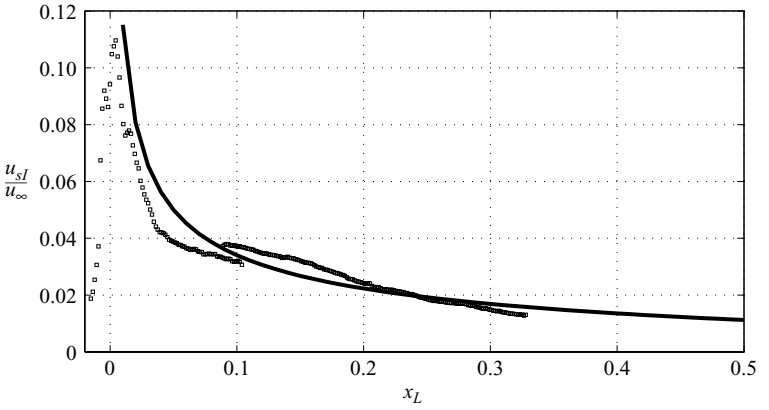

FIGURE 6. Velocity deficit along the centreline $\hat{u}_{sI}$ normalized with the ambient velocity u_∞. Analytical solution in the case of dominance of free turbulence (case I) for $S = 0.02$ (continuous line). Symbols denote experimental data (Carmer 2005) of a vortex street-like wake in a shallow flow with $S = 0.02$ (Carmer 2005).

where $F = 0.25$ is a constant determined by Tennekes & Lumley through a comparison with available experimental data (cf. Tennekes & Lumley 1977, p. 116). Hence, A and B can be estimated by imposing that (3.25) reduces to the above solution in the limit of negligible bottom friction. However, solution (3.25) presents a singularity in the limit of vanishing bottom friction; hence, a Taylor expansion of equation (3.25) is introduced:

$$l(x) = \sqrt{-B + 2Ax} - \frac{1}{16}\frac{Ax^2}{\sqrt{-B + 2Ax}} f + O(f^2), \tag{3.28}$$

which, for $f \to 0$, reduces to

$$\lim_{f \to 0} l(x) = \sqrt{-B + 2Ax}. \tag{3.29}$$

We note that (3.29) reproduces (3.27) provided that $B = 0$.

Furthermore, using the stability number S, (3.25) and (3.26) can be given the following form

$$\tilde{l}_I(x_L) = \sqrt{\frac{4A\,[1 - \exp(-x_L)]}{SD}}, \qquad \tilde{\hat{u}}_{sI}(x_L) = \frac{\exp(-x_L)A}{Dm\tilde{l}_I}, \tag{3.30}$$

where $\tilde{l}_I$ is the transverse wake width normalized with the cylinder diameter D and $\tilde{\hat{u}}_{sI}$ is the velocity deficit, normalized with the ambient velocity u_∞.

According to the standard fitting procedure used for self-similar solutions (see Tennekes & Lumley 1977) the constant A is determined through the comparison of solution (3.30) with the experimental data of Carmer (2005). Such comparison, reported in figure 5, reveals that the best match is obtained if we set $A = D/32$.

The resulting solution then reads:

$$\tilde{l}_I(x_L) = \sqrt{\frac{[1 - \exp(-x_L)]}{8S}}, \qquad \tilde{\hat{u}}_{sI}(x_L) = \frac{\exp(-x_L)}{32m\tilde{l}_I}. \tag{3.31}$$

The analytical solution for u_s (continuous line) compares satisfactorily with experimental data for a vortex street-like wake ($S = 0.02$) as shown in figure 6.

Once the above solutions have been obtained, the transverse velocity profile can be derived from (3.18) which is now rewritten in the following form:

$$\frac{\mathrm{d}^2\varphi}{\mathrm{d}\zeta^2} + \frac{m}{\kappa}\zeta\frac{\mathrm{d}\varphi}{\mathrm{d}\zeta} + \frac{m}{\kappa}\varphi = 0. \tag{3.32}$$

Equation (3.18) has the non-trivial solution:

$$\varphi(\zeta) = \exp\left(-\frac{1}{2}\mu\zeta^2\right), \tag{3.33}$$

where

$$\mu = \frac{m}{\kappa}. \tag{3.34}$$

The constant μ can be set arbitrarily since its value defines the transverse length l, which has been left unspecified. If we set $\mu = 1$, we obtain

$$\varphi(\zeta = 1) = \mathrm{e}^{-1/2} \cong 0.61,$$

which implies that l is defined as the distance from the centreline for which the velocity deficit is 61 % of the deficit along the centreline.

The constant m can be estimated recalling the definition of momentum deficit:

$$\mathscr{M} = \int_{-\infty}^{+\infty} u u_s h_\infty \,\mathrm{d}y \simeq \int_{-\infty}^{+\infty} u_\infty u_s h_\infty \,\mathrm{d}y, \tag{3.35}$$

where the contribution associated with the longitudinal turbulent flux and the term proportional to u_s^2 have been neglected. Using (3.2), (3.25), (3.26) and (3.33), we obtain:

$$m = \left(\frac{\sqrt{2\pi\kappa}\,u_\infty^2 D h_\infty}{32\mathscr{M}_0}\right)^{2/3}. \tag{3.36}$$

The constant κ has been determined by fitting experimental data for the transverse velocity profiles with the exponential function (3.33). Results of the above procedure are reported in figure 7 for a vortex street-like wake ($S = 0.02$). Note that sufficiently far from the obstacle, i.e. in the region of validity of this analytical formulation, κ seems to assume a constant value roughly equal to 2.

The resulting velocity profile in the transverse direction (3.33) is in good agreement with experimental data for shallow wakes behind cylindrical obstacles (see figure 8). No major discrepancies at the wake outer edge, typically characterizing planar turbulent wakes immersed in an irrotational flow, can be observed for the shallow wake at hand. The outer flow is not irrotational, but turbulent because of bottom friction effects. However, this cannot be so easily explained and thus it remains an open issue.

Equation (3.34) suggests that ν_t must decrease with x, because so does the product $u_s l$. This is shown in figure 9: sufficiently away from the obstacle, the turbulent viscosity decreases until it vanishes as the effect of the turbulent wake becomes negligible. Furthermore, the Reynolds number built with u_s and l does not remain constant: it exponentially decreases with the product $u_s l$. This means that the wake in the case of free turbulence decreases in the x-direction and the flow asymptotically reaches the conditions of the turbulent ambient region, unlike the case of a plane unbounded wake where the Reynolds number remains constant (cf. Tennekes & Lumley 1977).

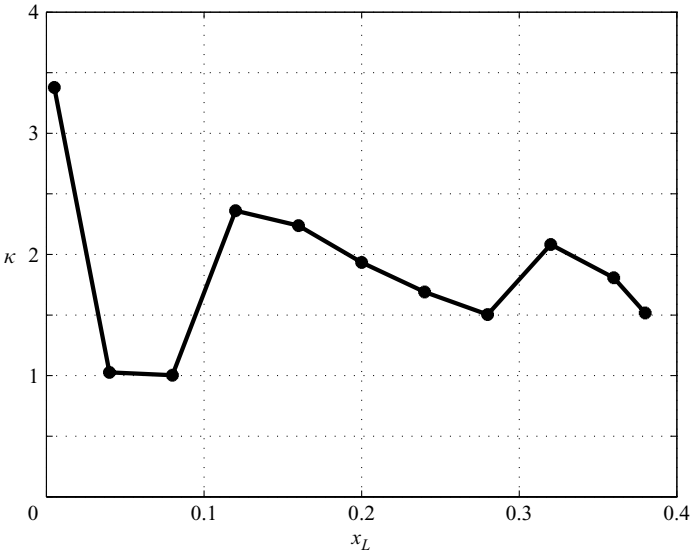

FIGURE 7. The constant κ for a vortex street-like wake ($S = 0.02$) behind a circular cylinder in shallow flows.

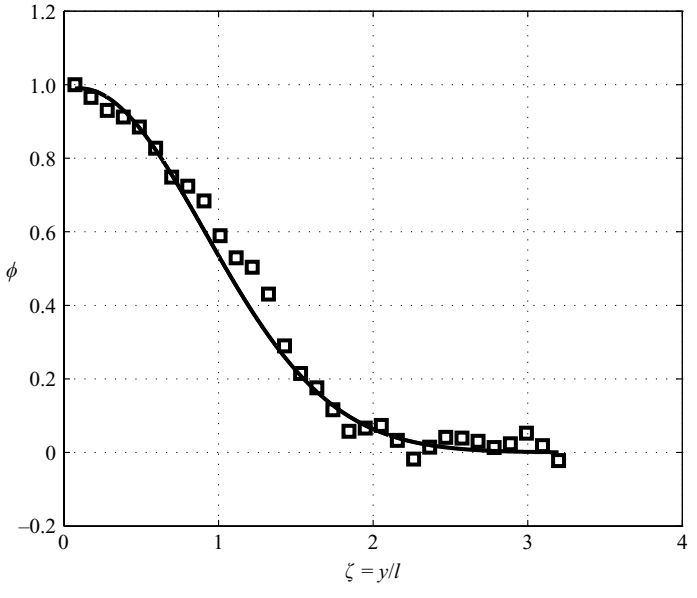

FIGURE 8. Comparison between the analytical solution for the transverse velocity profile $\varphi(\zeta)$ obtained for the case of dominance of free turbulence and experimental data (Carmer 2005) of a vortex street-like wake in shallow flow ($S = 0.02$).

3.4. *Self-similarity and mean velocity profile: dominance of wall turbulence (case II)*

For large values of bottom roughness, turbulence production in shallow wakes is essentially caused by the bottom friction, while vorticity induced by the wake flow becomes negligible. This happens in the extreme far-wake region, i.e. for $x_L \gg 1$

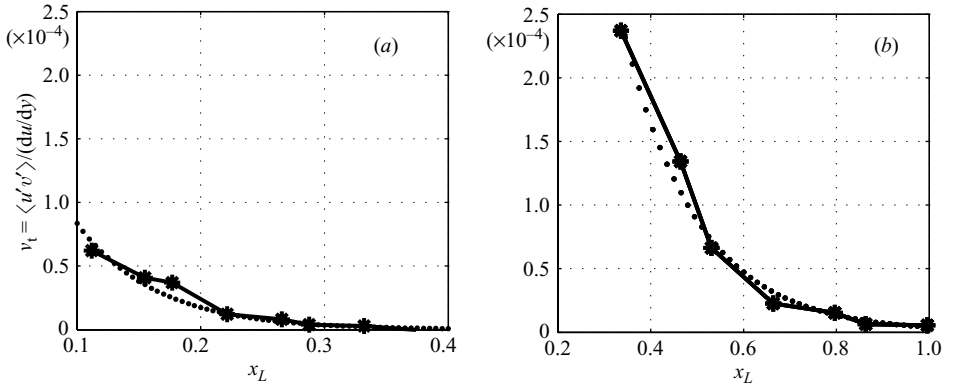

FIGURE 9. The turbulent viscosity ν_t for two vortex street-like wakes behind a circular cylinder in shallow flows. (*a*) $S = 0.02$; (*b*) $S = 0.06$. The values are obtained from experimental data (Carmer (2005)) and are calculated as the ratio between the measured Reynolds stresses and the velocity gradient between two longitudinal sections. Experimental data are interpolated through exponential functions (dots).

(cf. figure 4). In this case, the velocity and length scales of the kinematic turbulent viscosity can be defined as in the classical wall-law, such that ν_t takes the following form:

$$\nu_t = \alpha u_\infty h_\infty. \tag{3.37}$$

Furthermore, the momentum flux due to turbulent fluctuations can be given in the form

$$-\frac{\partial(\overline{u'v'})}{\partial y} = -\frac{1}{l}\frac{\partial}{\partial \zeta}\left[\frac{\nu_t}{l}\frac{\partial u_s}{\partial \zeta}\right] = -\frac{1}{l^2}\alpha u_\infty h_\infty \hat{u}_s \frac{\mathrm{d}^2\varphi}{\mathrm{d}\zeta^2}. \tag{3.38}$$

Substituting into (3.11), it follows that

$$-\left[\frac{l^2}{\hat{u}_s h_\infty}\frac{\mathrm{d}\hat{u}_s}{\mathrm{d}x} + \frac{f l^2}{8h_\infty^2}\right]\varphi + \left[\frac{l}{h_\infty}\frac{\mathrm{d}l}{\mathrm{d}x}\right]\zeta\frac{\mathrm{d}\varphi}{\mathrm{d}\zeta} = -\alpha\frac{\mathrm{d}^2\varphi}{\mathrm{d}\zeta^2}. \tag{3.39}$$

Self-similarity requires that the terms in the square brackets be constant, i.e. that:

$$\frac{l^2}{\hat{u}_s h_\infty}\frac{\mathrm{d}\hat{u}_s}{\mathrm{d}x} + \frac{f}{8h_\infty^2}l^2 = t, \tag{3.40}$$

$$\frac{l}{h_\infty}\frac{\mathrm{d}l}{\mathrm{d}x} = r. \tag{3.41}$$

The latter condition leads to the following expression for $l(x)$:

$$l_{II}(x) = \sqrt{2rh_\infty x + 2A'}. \tag{3.42}$$

Substituting (3.42) into (3.40), an ordinary differential equation for $\hat{u}_s$ is obtained:

$$\frac{(2rh_\infty x + 2A')}{\hat{u}_s}\frac{\mathrm{d}\hat{u}_s}{\mathrm{d}x} + \frac{f}{8h_\infty}(2rh_\infty x + 2A') = th_\infty, \tag{3.43}$$

whose solution is

$$\hat{u}_{sII}(x) = B'\exp\left(-\frac{f}{8h_\infty}x\right)(rh_\infty x + A')^{t/2r}, \tag{3.44}$$

where A' and B' are integration constants which have to be determined through comparison with experimental data.

The same arguments used for case I suggest that the solution for φ can be obtained only if we set $t/r = -1$; it follows that (3.39) can then be rewritten as:

$$\frac{\mathrm{d}^2\varphi}{\mathrm{d}\zeta^2} + \frac{r}{\alpha}\zeta\frac{\mathrm{d}\varphi}{\mathrm{d}\zeta} + \frac{r}{\alpha}\varphi = 0, \tag{3.45}$$

whose non-trivial solution is

$$\varphi(\zeta) = \exp\left(-\frac{1}{2}\mu\zeta^2\right), \tag{3.46}$$

where

$$\mu = \frac{r}{\alpha}. \tag{3.47}$$

Note that (3.46) coincides with (3.33); hence, as in § 3.3, the value of μ can be arbitrarily chosen. Furthermore, the constant α should be determined experimentally; though no experimental data are presently available.

As for the case of dominant free turbulence, ν_t is constant along the longitudinal direction, because the product $u_\infty h_\infty$ is. Furthermore, the Reynolds number set in terms of u_s and l decreases in the longitudinal direction.

3.5. *Comparison with unbounded wakes and discussion*

In the present work, an analytical solution for shallow-wake flows has been derived including the effects of bottom friction and acceleration due to gravity. Its structure depends on the relevant characteristic scales of the problem; however, the momentum deficit has invariably been found to decay in the longitudinal direction owing to bottom friction.

Two limiting cases have been considered which correspond to a different choice of the closure relationship for turbulent shear stress: the former limit is approached when wake turbulence dominates over the wall turbulence, which is the case in the nearer far-wake region, whereas in the latter, the phenomena is dominated by boundary-layer effects and happens in the extreme far-wake region. In the former case, the analytical solution degenerates, in the frictionless asymptotic limit, into the solution obtained by Tennekes & Lumley (1977) which is valid for unbounded wakes with a perfectly smooth bottom.

The present results suggest that the flow structure of shallow wakes behind cylindrical obstacles displays several distinctive features with respect to that characterizing unbounded wake flows. The above differences are highlighted in the comparison reported in table 1.

A first noticeable difference is the behaviour of the momentum deficit $\mathscr{M} = \int_{-\infty}^{+\infty} u u_s l \, \mathrm{d}y$ (cf. § 3.1), which follows an exponentially decreasing trend in the longitudinal direction, while it remains constant in an unbounded wake. It could be argued that such behavior should imply a production of *total momentum*. However, the reduction of the momentum deficit in shallow wakes does not lead to a momentum growth, but is dissipated by bottom friction. On the other hand, the dissipative effect of the bottom friction is reduced by the counteracting effect of the gravitational term (cf. (2.18)); dimensional analysis suggests that the above effects have the same order of magnitude.

Furthermore, the transverse displacement of shallow wakes is smaller than that of an unbounded wake (cf. equation (3.30)). In fact, bottom friction inhibits the

Description	Shallow wake: case II	Shallow wake: case I	Unbounded wake
Validity	$x_L \geqslant 1$	$x_L \leqslant 1$	$f = 0$
Momentum deficit	Decreasing	Decreasing	Constant
Transverse wake length	$\sim x^{1/2}$	$\sim(1-e^{-x})^{1/2}$	$\sim x^{1/2}$
Velocity deficit	$\sim \dfrac{e^{-x}}{x^{1/2}}$	$\sim \dfrac{e^{-x}}{(1-e^{-x})^{1/2}}$	$\sim x^{-1/2}$
Velocity profile	Gaussian	Gaussian	Gaussian
Closure turbulent term	$\nu_T = \alpha u_\infty h_\infty$	$\nu_T = \kappa \hat{u}_s l$	$\nu_T = -\hat{u}_s l \mathscr{F}(\zeta)$
Turbulent viscosity	Constant	Decreasing with x	Constant
$Re_T = \dfrac{\hat{u}_s l}{\nu_T}$	Constant	Constant	Constant
$Re = \dfrac{\hat{u}_s l}{\nu}$	Decreasing with x	Decreasing with x	Constant

TABLE 1. Comparison between the present analytical solutions for a shallow wake and that corresponding to an unbounded wake.

development of two-dimensional structures, which are mainly responsible for the spreading of the wake, since it subtracts turbulent energy from the large scales. In other words, the exchange of momentum deficit between the ambient region and the wake zone, owing to turbulent fluctuations associated with two-dimensional coherent structures, is hampered by bottom friction. Moreover, the decrease of the velocity deficit in a shallow wake is faster than that of an unbounded wake (cf. equation (3.30)), which implies that in shallow wakes, the region characterized by velocity deficit does not persist over large distances far from the body. This finding also indicates that bottom friction tends to stabilize the flow, improving the energy transfer from the large to the small scales. In this respect, friction plays a role in the stability of shallow flows similar to that played by viscosity in the transition between laminar and turbulent states in an unbounded flow.

The present analysis also shows that shallow wakes belong to that class of flows for which a self-similarity assumption can be stipulated, both in the case of dominant free turbulence and in the case of dominant friction. Solutions (3.33) and (3.46) differ in that the above limiting conditions are characterized by different length and velocity scales.

Equation (3.34) also states that, for a shallow wake, the turbulent viscosity in the case of dominant free turbulence is decreasing in the longitudinal direction, as the product $\hat{u}_s l$, while it remains constant both for the case of dominant wall turbulence and for an unbounded wake. As a consequence, in the case of dominant free turbulence, the Reynolds number defined in terms of the velocity deficit, the transverse length scale of the wake and the kinematic viscosity also decreases in the longitudinal direction. On the contrary, the turbulent Reynolds number set in terms of the turbulent kinematic viscosity is constant for both shallow wakes and for unbounded wakes.

4. Summary

An analytical study of shallow-wake flows is proposed, and general solutions for the characteristic scales governing this problem are obtained, including the effect of bottom friction and of the acceleration due to gravity. The solution is obtained by solving, through a simplified procedure, the St Venant equations of motion. An

expression for the momentum deficit is derived and the solution shows a decay in the longitudinal direction owing to friction. Two limiting cases have been distinguished which correspond to different choices of turbulence closure. The first case, for which the wake turbulence dominates boundary-layer effects, is valid in the nearer far-wake region while the second limit is approached further downstream where the phenomenon is dominated by boundary-layer effects. Matching between the solutions valid in the asymptotic limits considered in our paper is obviously not possible, since in the former case (dominance of wake turbulence) the effect of the bottom friction related to the velocity deficit is discarded.

The presented solutions show that the velocity deficit decreases faster and the transverse dimension of the wake increases more slowly when compared to that of unbounded wakes. Furthermore, the momentum deficit exponentially decreases in the longitudinal direction owing to the roughness of the bed. The exchange of momentum deficit between the ambient region and the wake zone, owing to turbulent fluctuations of the two-dimensional coherent structures, is hampered by the bottom friction, which dissipates the turbulent kinetic energy of these structures. The dimensional analysis of the equations of motion shows the importance of the gravitational term, which has the same order of magnitude as the friction term.

A comparison with experimental data is also performed and a good match is found. For the case of wall turbulence dominance, a comparison with experimental data is not possible since such data are not available. In table 1, all the results are summarized.

Finally, it is worth noting that the analytical solution derived herein for the transverse structure of the velocity profile can be used as a suitable starting point to characterize further hydrodynamic properties of the wake flow, as well as to perform stability analysis of the wake flow such as those performed by Chen & Jirka (1997) or Socolofsky & Jirka (2004).

The authors would like to thank Carl F. von Carmer for making available experimental data and Kevin Tetz for proof-reading. Further acknowledgements go to the German Science Foundation (DFG Ji 18/4) for its support in conducting this research.

REFERENCES

Bearman, P. W. 1967 Investigation of the flow behind a two-dimensional model with blunt trailing edge and fitted with splitter plate. *J. Fluid Mech.* **21**, 241–255.

Berger, S. A. 1971 *Laminar Wakes.* Elsevier. 335 pp.

v Carmer, C. F. 2005 Shallow turbulent wake flows: momentum and mass transfer due to large-scale coherent vortical structures. Dissertationsreihe am Institut für Hydromechanik der Universität Karlsruhe (TH), 3-937300-63-5, 1439-4111, Universitätsverlag Karlsruhe, Germany.

Chen, D. & Jirka, G. H. 1995 Experimental study of plane turbulent wakes in a shallow water layer. *Fluid Dyn. Res.* **16**, 11–41.

Chen, D. & Jirka, G. H. 1997 Absolute and convective instabilities of plane turbulent wakes in a shallow water layer. *Fluid Dyn. Res.* **338**, 157–172.

Grubisic, V. & Smith, R. B. & Schar, C. 1995 The effect of bottom friction on shallow flow past an isolated obstacle. *J. Atmos. Sci.* **48**, 1985.

Huerre, P. & Monkewitz, P. A. 1990 Local and global instabilities in spatially developing flows. *Annu. Rev. Fluid Mech.* **22**, 473.

Hinze, J. O. 1975 Turbulence, McGraw-Hill. 2nd edn.

Jirka, G. H. 2001 Large scale flow structures and mixing processes in shallow flows. *J. Hydraul. Res.* **39-1**, 567–573.

Negretti, M. E. 2003 Analysis of the wake behind a circular cylinder in shallow water flows, pp. 70–80. Master Thesis, University of Trento.

Pope, S. B. 2000 *Turbulent Flows*. Cambridge University Press.

Schlichting, H. & Gersten, K. 2000 *Boundary Layer Theory*. Springer.

Socolofsky, S. A. & Jirka, G. H. 2004 Large scale flow structures and stability in shallow flows. *J. Environ. Engng Sci.* **3**, 451–462.

Stansby, P. K. 2003 A mixing-length model for shallow turbulent wakes *J. Fluid Mech.* **495**, 369–384.

Tennekes, H. & Lumley, J. L. 1977 *A First Course in Turbulence*. Cambridge MIT Press.

Tollmien, W. 1931 Grenzschicht Theorie. *Handbuch der Experimentalphysik,* vol. 4, part 1. Leipzig.

Williamson, C. H. K. 1996 Vortex dynamics in the cylinder wake. *Annu. Rev. Fluid Mech.* **28**, 477–539.